Eur. Phys. J. A (2016) **52**: 73
DOI 10.1140/epja/i2016-16073-6

THE EUROPEAN PHYSICAL JOURNAL A

Regular Article – Experimental Physics

The nuclear physics of the hydrogen burning in the Sun*

Alba Formicola[1,a], Pietro Corvisiero[2], and Gianpiero Gervino[3]

[1] INFN, Laboratori Nazionali del Gran Sasso, Assergi, via Acitelli 22, 67100 L'Aquila, Italy
[2] Dipartimento di Fisica, Università di Genova and INFN Genova, via Dedecaneso 33, 16144 Genova, Italy
[3] Dipartimento di Fisica, Università di Torino and INFN Torino, via Giuria 1, 10125 Torino, Italy

Received: 31 July 2015 / Revised: 23 December 2015
Published online: 5 April 2016 – © Società Italiana di Fisica / Springer-Verlag 2016
Communicated by C. Broggini

The Luna Collaboration dedicates this paper to the memory of Prof. Roberto Bonetti and Dr. Alberto Lemut. We deeply miss their help and advice, and their friendship.

Abstract. Underground nuclear astrophysics focuses its efforts towards a deeper knowledge of the nuclear reactions that rule stellar evolution processes and enable the synthesis of the elements of the periodic table. Deep underground in the Gran Sasso laboratory, the cross-sections of the key reactions of the hydrogen burning have been measured right down to the energies of astrophysical interest. The main results obtained by the LUNA Collaboration are reviewed, and their contributions to the solution of the solar neutrino problem and to the age of the globular cluster are discussed.

1 Introduction

All the elements of the periodic table, with the exception of hydrogen, helium and lithium which started to be produced in the very first minutes after the Big Bang, have their only origin in the thermonuclear reactions taking place inside the stars, which can be seen as enormous cauldrons lost in the cosmos. The aim of the nuclear astrophysics research project at LUNA, in the underground laboratories of Gran Sasso, is to improve the knowledge of the reaction mechanisms that rule the transmutation of the chemical elements and provide the energy that keeps the stellar cauldrons at work. The key parameter of the reaction mechanism is the cross-section that should be measured at stellar energies. At such energies, cross-sections are extremely small: experimental measurements need an extremely low-background environment, this request is fulfilled inside the Gran Sasso laboratory [1,2]. In this paper the main results achieved by the LUNA Collaboration in the hydrogen burning process will be presented. The contribution of LUNA measurements to the solution of the solar neutrino problem and to the carbon-nitrogen-oxygen (CNO) cycle will also be outlined.

* Contribution to the Topical Issue "Underground nuclear astrophysics and solar neutrinos: Impact on astrophysics, solar and neutrino physics" edited by Gianpaolo Bellini, Carlo Broggini, Alessandra Guglielmetti.

[a] e-mail: formicola@lngs.infn.it

2 Neutrino and nuclear astrophysics

Casting a glance deep inside the nature of neutrino was the subject of many research efforts. The discovery of neutrino oscillations, which indirectly supports the assumption that neutrinos have a mass, put an end to the solar neutrino problem.

For more than 30 years, the missing solar neutrino flux was considered one of the most interesting problems in physics [3,4]. The need for physics beyond the standard electroweak model arose following a) confirmation of the solar model, which was achieved using helioseismology [5] to determine the interior sound speed, b) new solar neutrino experiments, and c) the exclusion of nuclear solutions, such as an undiscovered low-energy resonance in the ^{3}He(^{3}He, 2p)^{4}He, which represents the main termination of the pp chain.

In the Standard Solar Model (SSM), the p-p chain reactions are the dominant mechanism of neutrino production. The energy generation of the Sun proceeds either through the pp chain (99%) or the CNO cycles ($\approx 1\%$), see fig. 1. The Standard Solar Model is continuously improved and verified: additional knowledge came from Borexino, a detector which measured low-energy solar neutrinos in real time; in particular, for the first time it was able to determine the flux of proton-proton chain (pp) neutrinos [6]. The pp chain proceeds either through the ^{3}He(^{3}He, 2p)^{4}He or through the ^{3}He$(\alpha,\gamma)^7$Be. Neutrino fluxes from ^{7}Be

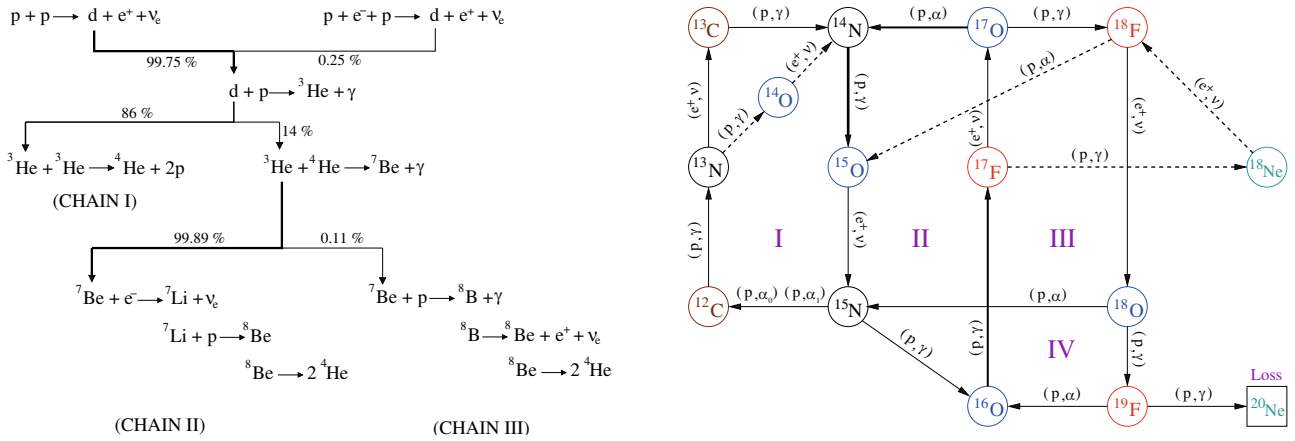

Fig. 1. Nuclear fusion reactions of the pp-chain (left panel) and the CNO cycle (right panel).

and ^{8}B decay are directly linked to the latter [4]. Its cross-section plays a crucial role: 9% uncertainty in its extrapolation down to the Gamow energy peak (23 keV) [7] contributes up to 8% [8] to the uncertainty in the evaluated fluxes for solar ^{7}Be and ^{8}B neutrinos. The flux of solar ^{8}B neutrinos has been measured in the SNO and SuperKamiokande detection set-ups [9,10], with a total experimental uncertainty down to 3.5% [10]. The predictions for CNO neutrino fluxes are not so precise because the CNO fusion reactions are not studied as efficiently as the p-p reactions [7], and because the Coulomb barrier is higher for the CNO reactions, implying a greater sensitivity to details of the solar model [4]. The most important processes that are believed to produce solar neutrinos within the CNO cycle are [11]

$$^{13}\mathrm{N} \rightarrow {}^{13}\mathrm{C} + e^+ + \nu \quad (Q \leq 1.199\,\mathrm{MeV}), \tag{1}$$

$$^{15}\mathrm{O} \rightarrow {}^{15}\mathrm{N} + e^+ + \nu \quad (Q \leq 1.732\,\mathrm{MeV}), \tag{2}$$

$$^{17}\mathrm{F} \rightarrow {}^{17}\mathrm{O} + e^+ + \nu \quad (Q \leq 1.740\,\mathrm{MeV}), \tag{3}$$

where Q is the energy of the neutrino. The two neutrino fluxes $\phi(^{13}\mathrm{N})$ and $\phi(^{15}\mathrm{O})$ depend almost linearly on the astrophysical S-factor $S(E)$ of the $^{14}\mathrm{N}(\mathrm{p},\gamma)^{15}\mathrm{O}$ reaction. Therefore, this reaction is important to precisely constrain the CNO cycle in the SSM. The recent downward revision of the metal content of convective zones has generated interest for testing the SSM further. Indeed, the new metal abundances significantly alter the agreement between Standard Solar Model predictions and helioseismology [12] in the temperature region below the solar convective zone. CNO neutrinos play a key role in this study; their direct detection and identification will provide independent information on the core metallicity of the Sun.

3 LUNA pilot project: The ^{3}He(^{3}He, 2p)^{4}He reaction

The reactions contributing to the pp chain and CNO bicycle are shown in fig. 1.

Typically, cross-sections are measured at somewhat higher energies, where rates are larger and then extrapolated to the solar energies of interest. Corrections are also due to the differences in the screening environment of terrestrial targets and the solar plasma. The primordial Sun metal abundances are generally determined from a combination of photospheric and meteoritic abundances, while the initial ^{4}He/H ratio is adjusted to reproduce, after 4.6 Gyr of evolution, the modern Sun luminosity. The SSM predicts that, as the Sun evolves, the core He abundance increases, the opacity and core temperature rise, and the luminosity increases (by a total of about 44% over 4.6 Gyr). The details of this evolution depend upon a variety of model input parameters and their uncertainties: the photon luminosity $L_\odot$, the mean radiative opacity, the solar age, the diffusion coefficients describing the gravitational settling of He and metals, the abundances of specific key metals, and the rates of the nuclear reactions. If the various nuclear rates are precisely known, the competition between burning paths can be used as a sensitive diagnostic of the central temperature of the Sun. Neutrinos probe this competition, as the relative rates of the ppI, ppII, and ppIII cycles comprising the pp chain (fig. 1) can be determined from the fluxes of the pp/pep, ^{7}Be and ^{8}B neutrinos. This is one of the reasons why laboratory astrophysics efforts to provide precise nuclear cross-section data have been so closely connected with solar neutrino detection. In the LUNA first phase (the so-called "pilot project"), a 50 kV accelerator facility has been installed in the Laboratori Nazionali del Gran Sasso (LNGS), where the average flux of cosmic-ray muons is reduced by a factor 10^6 [13]. The Laboratory for Underground Nuclear Astrophysics (LUNA) was designed primarily for a renewed study of the ^{3}He(^{3}He, 2p)^{4}He reaction ($Q = 12.86$ MeV) in the energy range of the solar Gamow peak ($E_0 \pm \delta E_0 = 21.9 \pm 6.2$ keV) for a central star temperature of $T = 15.5 \cdot 10^6$ K. The reaction is included in the hydrogen burning pp chain [14], which is predominantly responsible for the energy generation and neutrino luminosity [3] of the Sun.

Previous measurements of this reaction existed at higher energies [15,16], far away from the Gamow peak but, still, the possibility of a narrow resonance at lower

energies [17,18] remained. The ^{3}He(^{3}He, 2p)^{4}He reaction is the termination of the ppI cycle and thus uncertainties in this cross-section played a prominent role in early speculations about a nuclear astrophysics solution to the solar neutrino problem [15,16]. As an increase in $S_{33}(E)$ would reduce the branchings to the ppII and ppIII cycles —thus also reducing the neutrino fluxes measured by Davis— the possibility of an undiscovered narrow resonance at energies beyond the reach of early experiments was first raised by Fetisov and Kopysov [18] and Fowler [17] in 1972. This motivated efforts to measure $S_{33}(E)$ at lower energies, stimulated the LUNA Collaboration in the 1990s to map the cross-section in the solar Gamow peak [19,20]. The main result is the completion of this program [21], extending measurements to the lower edge of the Gamow peak (16 keV), making $S_{33}(E)$ the most directly constrained S-factor within the pp chain. Briefly, the 50 kV accelerator facility consisted of a duoplasmatron ion source, an extraction and acceleration system, a double-focusing 90° analyzing magnet, a windowless gas-target system, and a beam calorimeter. The energy spread of the ion source was less than 20 eV, the plasma potential energy deviated by less than 10 eV from the voltage applied to the anode, and the emittance of the source was 2 cm rad eV$^{1/2}$ [19] The detection setup for the ^{3}He(^{3}He, 2p)^{4}He studies had to fulfill the following requirements:

- High absolute efficiency, in view of the expected reaction rates of about 1 event/day and less.
- High rejection of natural radioactivity in the detectors, in the target chamber facing the detectors, and from the surrounding rocks at LNGS (mainly γ).
- High rejection of electronic noise, in view of the needed running times of several weeks for each energy point.
- Clear separation of the reaction products from those of the competitive reaction ^{3}He(d, p)^{4}He (Q = 18.35 MeV), due to deuterium contamination in the ^{3}He beam (as HD^+ molecules of mass 3) and in the gas target.

This contaminant reaction has a cross-section one millionfold higher than that of ^{3}He(^{3}He, 2p)^{4}He at $E_{\rm lab}$ = 40 keV, mainly due to the barrier penetrability ratio P(d + ^{3}He)/P(^{3}He + ^{3}He) $\approx 10^6$, and thus extremely small deuterium contaminations (of the order 10^{-6}) could lead to sizable event rates. In order to optimize the detection setup and to understand the resulting spectra for quantitative analyses, a Monte Carlo program [22] was developed to simulate the experiment under realistic conditions. Setup consisted of four ΔE-E silicon detector telescopes (see fig. 2) placed inside the gas target in a box shape around the beam line flight. This configuration allowed, analyzing data in the E-ΔE plane, to disentangle protons emitted by the two above mentioned reactions (see fig. 3). With this setup configuration, a preliminary measurement performed in Bochum with the 450 kV accelerator turned out in full agreement with previous literature data [15,16,23].

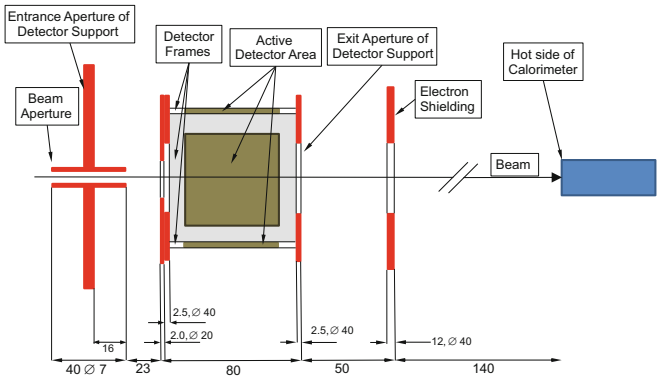

Fig. 2. Shematic view of the setup used at LNGS for the ^{3}He(^{3}He, 2p)^{4}He measurements.

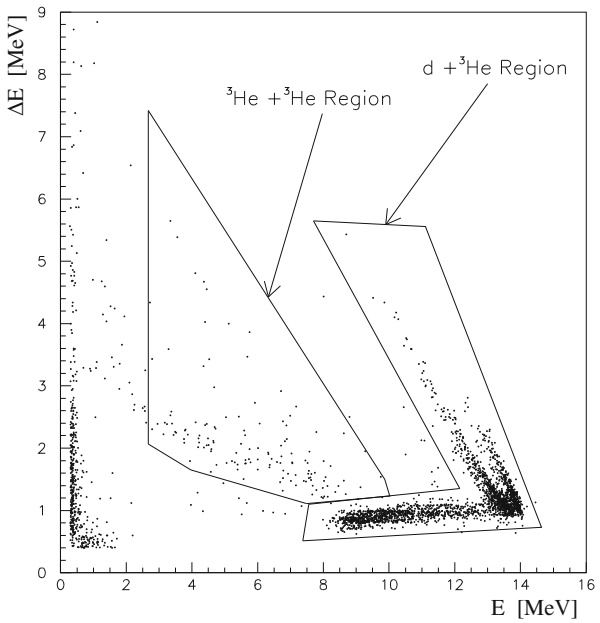

Fig. 3. Identification matrix of one ΔE-E telescope used in the ^{3}He(^{3}He, 2p)^{4}He measurements performed by the LUNA Collaboration.

Then, this reaction was measured in the underground Gran Sasso Laboratory in the c.m. energy interval 20 $\leq E_{cm} \leq$ 25 keV with the same setup. Later the reaction was measured down to E_{cm} = 16.5 keV with a modified, higher detection efficiency setup realized with eight Si detectors forming a double square box: in this case the signal was given by the proton-proton coincidence on couple of detectors [21]. The overall result is reported in fig. 4 together with the literature data of refs. [23] and [16]. Subsequently, Itahashi *et al.* [24] repeated this measurement in 2003 in the energy range 31 $\leq E_{cm} \leq$ 45 keV obtaining results in full agreement with LUNA [20,21]. A correction must be applied to the measured S-factor, due to the electron screening effect, sizeable at these low energies and clearly evident in fig. 4. In order to extract the $S(0)$ value, all the existing data between 16.5 and 1080 keV were fitted using

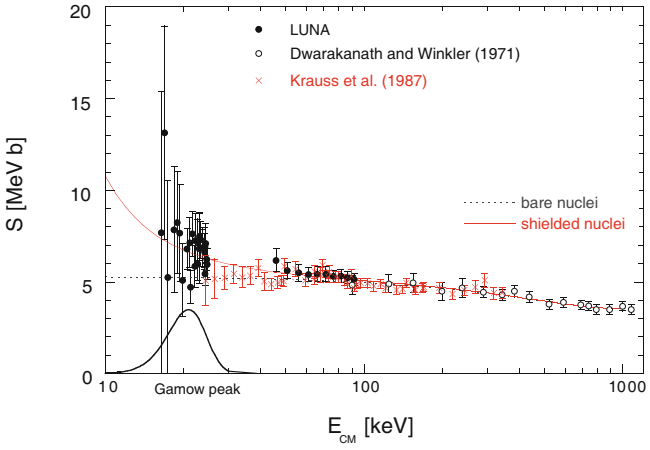

Fig. 4. (Color online) The ^{3}He(^{3}He, 2p)^{4}He S-factor from previous measurements and from LUNA. The lines show the fit to astrophysical factors for bare (dot-dotted line) and shielded (red line) nucleus. Also schematically shown is the solar Gamow peak region (black line).

Table 1. $S_b(E)$ factors and screening potential U_e.

$S_b(0)$ (MeV b)	$S_b'(0)$ (b)	$S_b''(0)$ (b/MeV)	U_e (eV)	$\chi^2/d.o.f.$
5.32 ± 0.08	-3.7 ± 0.6	3.9 ± 1.0	294 ± 47	0.86

these equations:

$$S_b(E) = S_b(0) + S_b'(0)E + \frac{1}{2}S_b''(0)E^2 \quad (4)$$

$$S_s(E) = S_b(E)\exp(\pi\eta U_e/E), \quad (5)$$

where S_b and S_s are the astrophysical S-factors for bare and shielded nuclei, respectively, η is the usual Sommerfeld parameter and U_e is the electron screening potential. $S_b(0)$, $S_b'(0)$, $S_b''(0)$ and U_e obtanied values are reported in table 1. The deduced screening potential value ($U_e = 294 \pm 47$ eV) is close to the adiabatic limit (240 eV). From these measurements it has been concluded that the ^{3}He(^{3}He, 2p)^{4}He cross-section increases at the thermal energy of the Sun as expected from the electron screening effect but does not show any evidence for a narrow resonance. The ratio of the pp/pep to ^{7}Be/^{8}B neutrino fluxes is important for future strategies to better constrain neutrino oscillation parameters and matter effects, through comparison of high-energy (matter influenced) and low-energy (vacuum) fluxes. The ratio of $S_{33}(E)$ to $S_{34}(E)$ enters in computing the energy losses via neutrino of the Sun, and thus influences the connection between the Sun photon luminosity and its total energy production.

4 High-accuracy measurement: The ^{3}He$(\alpha,\gamma)^7$Be reaction

The ^{3}He$(\alpha,\gamma)^7$Be (Q-value = 1.586 MeV) is a radiative capture reaction into the ground state or the first excited state ($E_x = 429$ keV) of ^{7}Be. The ground state of ^{7}Be decays by electron capture (EC) into ^{7}Li with a half-life of 53.22 ± 0.06 [25], populating the first excited state of ^{7}Li at $E_x = 478$ keV (later de-exciting to the ground state) with a branching ratio of about 10%. The LUNA research program on ^{3}He$(\alpha,\gamma)^7$Be was designed in order to exploit two different techniques. In the first approach direct α-capture γ-rays were detected (prompt γ method, see also the measurements reported in [26–33]), while, in the second one, the delayed ^{7}Be-decay γ-rays were counted (activation method, see [26,34–39]). Before the LUNA experiment, the average of the prompt data and of the activation data, covering a wide energy range, had an apparent discrepancy of about 9%. No satisfactory explanation was found: it could have been due either to systematic experimental errors (angular distribution, branching ratio effects, parasitic reactions producing ^{7}Be) or to the existence of a non-radiative capture ($E0$ monopole) [40]. The goal of LUNA was to supply high-accuracy data taken simultaneously at the same energy with both techniques. The reached accuracies were about 3% and 4% for the activation and prompt gamma measurements, respectively. The energies were chosen in order to reach higher precision at energies that are low enough to constrain the extrapolation down to solar Gamow window [41,42].

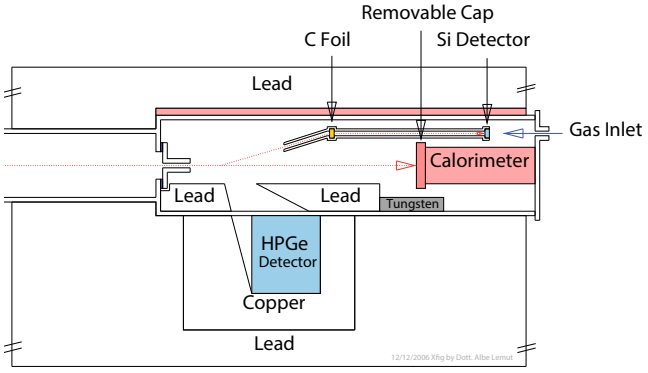

Fig. 5. Schematic view of the interaction chamber with the position of the HpGe detector and of the 100 μm silicon detector used for ^{3}He density monitoring.

4.1 Experimental results from prompt γ and activation measurements of ^{3}He$(\alpha,\gamma)^7$Be

The experiment has been carried out using the underground LUNA 400 kV accelerator [43] at the Gran Sasso National Laboratory. Three couples of cross-section values have been measured (prompt γ and activation) at $E_\alpha = 220, 250$, and 400 keV, few more energy points ($E_\alpha = 398, 350, 300$) have been measured only by the activation method [44]. A sketch of the interaction chamber is given in fig. 5, more details in [45]. Briefly, the α beam enters the ^{3}He windowless gas target [45] through a 7 mm diameter collimator and is stopped on a removable copper disk that serves as the primary catcher for the produced ^{7}Be and also as the hot side of a calorimeter [46].

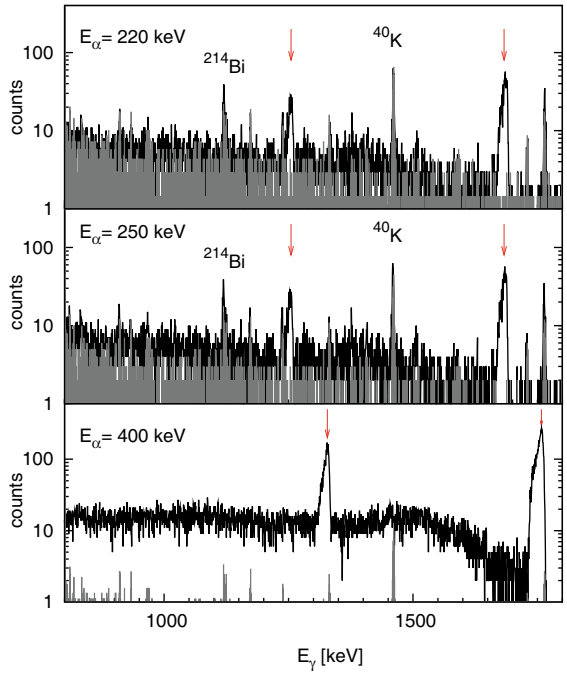

Fig. 6. γ-ray spectrum at $E_\alpha = 220, 250$, and 400 keV compared with natural laboratory background (in grey) normalized to beam measurement live times (respectively, 31.2 d, 21.3 d, and 4.8 d). Arrows indicate the primary transition peaks to the first excited state and to the ground state [45].

The detector and the shield (made by a castle of lead bricks completely surrounding the gas target) are enclosed in a sealed plastic box flushed with N_2 to reduce Rn and its daughters background. Thanks to the underground environment, the shielding suppression factor is better than five orders of magnitude for γ-rays below 2 MeV [47,48]. To minimize the systematic error due to angular distribution uncertainty, a lead collimator has been inserted inside the target chamber (fig. 5) to collect most of the γ-rays emitted at around 55° angle with the HpGe detector. The particular shape of this collimator was studied with the LUNA Monte Carlo (MC) code [49] taking into account the extended target effect and the detector solid angle. The spectra collected at $E_\alpha = 220, 250$, and 400 keV, with a total charge of 637, 407, and 113 C, respectively, are shown in fig. 6. Beam-induced γ-ray background has been measured with ^{4}He gas inside the target at $E_\alpha = 400$ keV (worst case): no difference with laboratory background has been observed. In order to compute detection efficiency, the coefficients of the Legendre polynomial expansion of the γ-ray angular distribution were linearly extrapolated to our energies from the curves reported in [50] and are in agreement with the theoretical predictions in [51]. A global uncertainty of 2.5% on the detection efficiency, which is the major contribution to the total error of the prompt γ method, has been estimated [50]. On the other hand, the activation method is based on the fact that, when α beam enters the ^{3}He gas target, ^{7}Be nuclei are produced and are implanted into the removable calorimeter copper cap. Calculations for the straggling of the α beam, for the production of ^{7}Be nuclei in the ^{3}He gas and for the emission cone of ^{7}Be (opening angle 1.8°–2.1°) have been carried out using both GEANT4 [52] and SRIM-like multiple scattering process [53] simulation. After each irradiation run, the cap was dismounted and put at counting in the LNGS underground low-counting facility [54]. To obtain a precise efficiency calibration, three homogeneous ^{7}Be sources of activity within 200–800 Bq and of 8 mm active diameter were prepared through the ^{7}Li(p, n)^{7}Be reaction using the 700 keV proton beam of MTA ATOMKI Van de Graaff accelerator at Debrecen (Hungary). Owing to the relatively low activities of the ^{7}Be implanted caps, random coincidence, summing effect and dead-time correction were fully negligible (see [55] for more details). Since we have simultaneously used the same beam and target for both methods, some systematic uncertainties (beam intensity, target density, and purity) cancel out in the comparison between the two techniques. Results are shown in fig. 7 together with all available literature data. A total (statistical and systematical) accuracy of about 3% for the $S(0)$ value has been obtained from LUNA data: $S(0) = 0.567 \pm 0.018 \pm 0.004$ keV b, where the last uncertainty term takes into account the indetermination due to the theoretical model adopted for extrapolation to zero energy. No discrepancy emerged between LUNA prompt and activation data [45,44] and [49,55] data. For this set of energies an electron screening enhancement factor [56] of up to 1.016 has been calculated in the adiabatic limit [57], but no correction for electron screening was applied. Thanks to the recent experimental results, it is now possible to reduce the uncertainty on the predicted ^{8}B neutrino flux due to S_{34} from 7.5% to 2.4% and the total uncertainty, including astrophysical parameters, has been decreased from 12% to 10%. Similarly, the uncertainty on ^{7}Be predicted flux has been decreased from 9.4% down to 5.5%, being the contribution of S_{34} error reduced from 8% to 2.5% [45,44]. deBoer *et al.* [58] in 2014, performed a global R-Matrix fit using ^{3}He$(\alpha,\gamma)^7$Be data (including the higher energy data from the European Recoil separator for Nuclear Astrophysics (ERNA) given in [59]), as well as scattering data leading to $S(0) = 0.542 \pm 0.011$(MC fit) $\pm$ 0.006(model)$^{+0.019}_{-0.011}$(phase shift) keV b. This work suggests to perform a measurement of the ^{3}He$(\alpha,\gamma)^7$Be reaction over an as wide as possible energy range using the same setup.

5 The ^{14}N(p, γ)^{15}O at low energy

The ^{14}N(p, γ)^{15}O reaction is the slowest of the CN cycle and, therefore, the key for understanding the timescale of the CNO cycles as well as the overall energy and neutrino production associated with CNO burning (see fig. 1). A series of new experiments using direct [60–65] and indirect approaches [66–70] has been carried out over the last 15 years. Here, we will mainly overview the LUNA achievements of the prompt γ radiation study testifying the enormous potential of underground environments [48]. In their pioneering work, Schröder *et al.* [71] found that

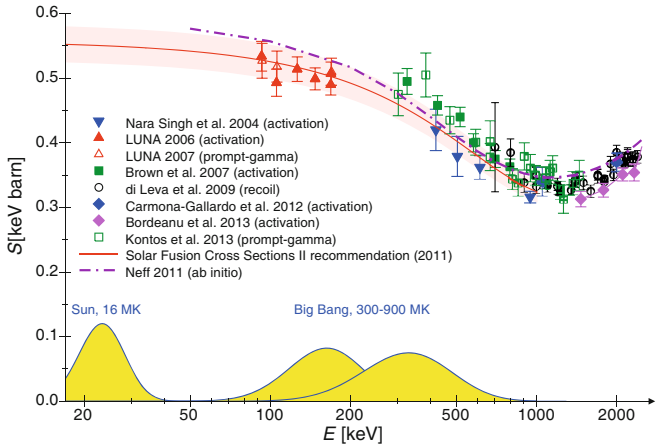

Fig. 7. (Color online) Overview of all available S-factor values for the $^{3}\mathrm{He}(\alpha,\gamma)^{7}\mathrm{Be}$ reaction. The yellow peaks are the reaction Gamow energy region for Sun and for Big Bang.

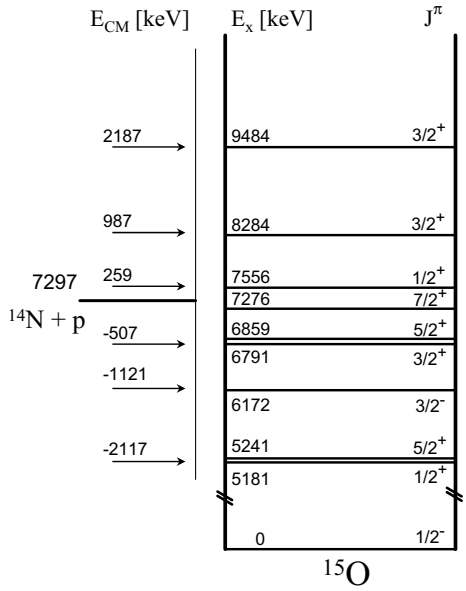

Fig. 8. The level structure of ^{15}O. (Above the $^{14}\mathrm{N}(\mathrm{p},\gamma)^{15}\mathrm{O}$ threshold only relevant states are shown.)

the reaction mechanism at low energies included contributions from resonant capture at $E_r = 259\,\mathrm{keV}$, direct capture, and capture from the tail of a sub-threshold resonance at $E_r = -507\,\mathrm{keV}$ (the resonance energies are in the center-of-mass system), corresponding to the known $E_x = 6791\,\mathrm{keV}$ state in ^{15}O, see fig. 8. The minimum energy explored by [71] for the ground state transition is about $E_{cm} = 252\,\mathrm{keV}$, well above the region of interest for the CNO burning in astrophysical conditions ($E_0 = 20$–$80\,\mathrm{keV}$, in core H-burning stars), so the values used in stellar model calculations were derived from extrapolations. In order to be reliable, such extrapolations must be more effectively constrained by as much experimental information as possible. The LUNA Collaboration measured the $^{14}\mathrm{N}(\mathrm{p},\gamma)^{15}\mathrm{O}$ reaction rate at low energies using the 400 keV accelerator [43] in two phases.

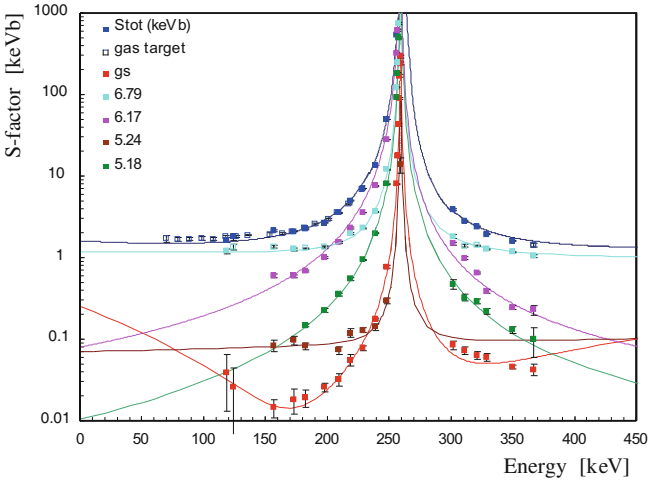

Fig. 9. (Color online) Astrophysical S-factor of $^{14}\mathrm{N}(\mathrm{p},\gamma)^{15}\mathrm{O}$ obtained at LUNA. Filled-in data points are from the HpGe and titanium nitride solid target setup [60,61], where each capture amplitude involved in the transitions to all bound states of ^{15}O has been detected. Open symbols are from the high-efficiency setup (BGO + gas target) [62,63], where the summing peak has been detected. The solid lines correspond to the R-matrix fit from [61].

The first phase was a low efficiency but high-energy resolution experiment [60] which was extended to energies down to $E_{cm} = 130.7\,\mathrm{keV}$. Using a high-purity germanium detector and titanium nitride solid target, information about the single contributions were derived. Later on, a second phase was realized using a high-efficiency but low-energy resolution 4πBGO summing detector (70% efficiency) in combination with a windowless gas target system. The two approaches were complementary and with the second phase experiment a lower energy limit of $E_{cm} = 70\,\mathrm{keV}$ was reached. As a disadvantage, only the total cross-section of the reaction was obtained. In the first phase, the $^{14}\mathrm{N}(\mathrm{p},\gamma)^{15}\mathrm{O}$ cross-section has been investigated in a wide energy range from $E_p = 140$ to $400\,\mathrm{keV}$ (or effective center-of-mass energy $E_{cm} = 120$ to $370\,\mathrm{keV}$), the measurements of the excitation function have been carried out using thick TiN targets on Ta backing. The mean distance between the target and the front face of the HpGe detector was 1.5 cm to guarantee a high detection efficiency. On the other hand, the price for this close geometry was a significant correction for the summing-in effect in all the observed ground state yields: this was a limit for the achievable precision. The data provide information on the capture amplitudes involved in the transitions to all bound states of ^{15}O (see fig. 9). The LUNA R-matrix fits based on the LUNA data and data in [71], which have been corrected for the summing-in effect, yield a total S-factor: $S_{\mathrm{tot}}\ (0) = 1.61 \pm 0.08\,\mathrm{keV\,b}$ [60] (the error 0.08 keV b is statistical only). The present result is in good agreement with [67] and [65] but differs in the weight of the contributions from the various transitions [61]. In the second project performed by the LUNA Collaboration [62,63] the total cross-section was determined. In this experiment

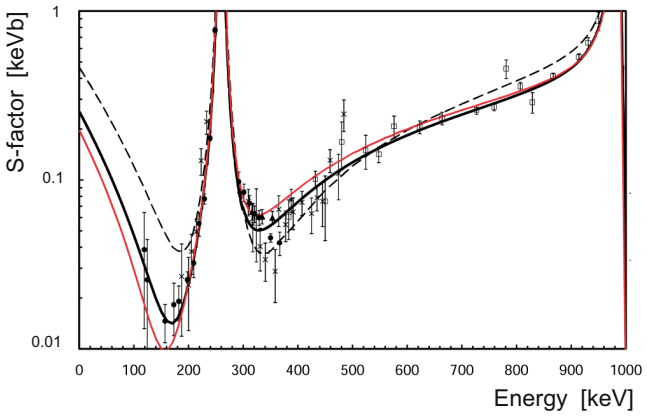

Fig. 10. (Color online) Astrophysical S-factor of $^{14}\mathrm{N}(\mathrm{p},\gamma)^{15}\mathrm{O}$ for the ground-state transition. Filled circle are data from [61], filled triangle [64], crosses [65] and open square [71]. R-matrix fit done in: [61] solid black line; [65] dashed line; [2] and [75] thin red line. The red fit takes into account data with small summing effects: *i.e.* [64] and in part [71].

the accelerator delivered a proton beam to a differentially pumped nitrogen windowless gas target. The γ-rays were detected by a 4πBGO summing crystal described elsewhere [46]. This experiment covered an energy range from 70 to 228 keV, with typically 3% (at most 10%) statistical and 5% (at most 7%) systematic uncertainty. For the first time, precision cross-section data have been obtained directly at energies of hydrogen burning in AGB stars. The resonance strength of the 259 keV resonance has been remeasured obtaining very good agreement with [61]. The total $S(E)$ factor from both solid and gas target set-ups is shown in fig. 9. An additional experiment was performed by the LUNA Collaboration in 2008 [64] at three (317.8, 334.4, and 353.3 keV) center-of-mass energies using again solid titanium nitride targets but a Clover composite germanium detector. The selected energies were located in a region where a sensitive minimum of R-matrix fits was observed [72] and the resonant contribution from the tail of the 259 keV resonance was limited. The experimental problem of the previous high summing-in correction for the ground state capture γ-rays [60,61] was solved by using this Clover detector: the systematic uncertainty due to the true coincidence summing-in correction was not larger than 30%. A new R-matrix fit has been performed which confirmed the previous LUNA result [61] for the capture to the ground state of ^{15}O. The combined data set of LUNA led to a rate reduction of a factor of 2, which increased the age of the oldest globular clusters, as derived from the turnoff luminosity, by about 0.7–1 Gyr with respect to the current estimates [73]. Furthermore, the analysis in [74] and [73] were partly based on the results of this revised reaction rate and led to the conclusion that the solar neutrino flux from CNO cycle is reduced by a factor of 2. All LUNA data allow improved extrapolations of the low-energy cross-sections using R-matrix calculations [60, 61] and removing the uncertainties discussed in previous extrapolations [72]. In spite of this major experimental effort, the Gamow peak for core H-burning stars is still well below the low-energy limit of direct γ-ray measurements. In particular, the cross-section here displayed as the astrophysical S-factor for the ground-state transition (fig. 10) is still insufficiently constrained by a good global fit of all available data. As obvious from the various fit curves in fig. 10 small systematic deviations on the high-energy side of the $E_r = 259$ keV resonance have a significant effect on the low-energy extrapolation, not yet constrained by the experimental data. A new and comprehensive study of the $^{14}\mathrm{N}(\mathrm{p},\gamma)^{15}\mathrm{O}$ reaction will need to cover a wide energy range. This kind of project has been submitted to INFN and involves both LUNA accelerators: the existing LUNA 400 kV machine as well as the future LUNA 3.5 MV facility. The combination of both systems will allow to cover the necessary energy range with a sufficient overlap and without any hole between 200 keV and 1.5 MeV. In order to obtain new information on this reaction, complete angular distributions must be determined over the entire energy range. In conclusion, with a new study of the $^{14}\mathrm{N}(\mathrm{p},\gamma)^{15}\mathrm{O}$ reaction at the future LUNA-MV facility it appears feasible to reach a precision necessary for further in-depth tests of the SSM. In the most updated SSM calculation, the present precision of the $^{14}\mathrm{N}(\mathrm{p},\gamma)^{15}\mathrm{O}$ cross-section is 7.2% (*i.e.* $S_{1,14}(0) = 1.66 \pm 0.12$ keV b) and, as a consequence, the uncertainties due to the $S_{1,14}$ and $S_{1,7}$ (7.7%) are dominating the SSM uncertainties for the nuclear rates [76]. Presently, a solar abundance problem is present: if the recently measured low metallicity values [77] are used as inputs in the SSM instead of the values reported in [78], then SSM predictions are no more in agreement with helioseismology data. Given the existing uncertainties on the astrophysical factors $S_{1,7}$ and $S_{1,14}$, a measurement of ^{15}O neutrinos with 10% uncertainty would allow a determination of the core C+N abundance with an uncertainty of about 15% [79]. We emphasize that the measurement of the core metallicity will provide an important test of a key SSM assumption: the solar surface metallicity is consistent with the core metallicity, *i.e.* the Sun was homogeneous when entering the main sequence.

The authors would like to express their thanks to S. Zavatarelli, H. Costantini, C. Rossi Alvarez, M. Marta, F. Terrasi, C. Rolfs and H.P. Trauttvetter for their work and support in the LUNA Collaboration.

References

1. C. Broggini *et al.*, Annu. Rev. Nucl. Part. Sci. **60**, 53 (2010).
2. H. Costantini *et al.*, Rep. Prog. Phys. **72**, 086301 (2009).
3. J.N. Bahcall, M.H. Pinsonneault, Rev. Mod. Phys. **64**, 885 (1992).
4. J.N. Bahcall, A.M. Serenelli, S. Basu, Astrophys. J. **621**, L85 (2005).
5. S. Basu, H.M. Antia, Phys. Rep. **457**, 217 (2008).
6. Borexino Collaboration, Nature **512**, 383 (2014) doi: 10.1038/nature13702.
7. E. Adelberger *et al.*, Rev. Mod. Phys. **70**, 1265 (1998).

8. J.N. Bahcall, M.H. Pinsonneault, Phys. Rev. Lett. **92**, 121301 (2004).
9. B. Aharmim *et al.*, Phys. Rev. C **72**, 055502 (2005).
10. J. Hosaka *et al.*, Phys. Rev. D **73**, 112001 (2006).
11. L. Ludhova, *Experimental data on solar neutrinos*, contribution to this Topical Issue.
12. A.M. Serenelli *et al.*, Astrophys. J. **705**, L123 (2009).
13. MACRO Collaboration, Phys. Lett. B **249**, 149 (1990).
14. V. Castellani, S. Degl'Innocenti, G. Fiorentini, Astron. Astrophys. **271**, 601 (1993).
15. M.R. Dwarakanath, H. Winkler, Phys. Rev. C **4**, 1532 (1971).
16. M.R. Dwarakanath, Phys. Rev. C **9**, 805 (1974).
17. W.A. Fowler, Nature **238**, 24 (1972).
18. V.N. Fetisov, Y.S. Kopysov, Nucl. Phys. A **239**, 511 (1975).
19. U. Greife *et al.*, Nucl. Instrum. Methods Phys. Res. A **350**, 327 (1994).
20. M. Junker *et al.*, Phys. Rev. C **57**, 2700 (1998).
21. R. Bonetti *et al.*, Phys. Rev. Lett. **82**, 5205 (1999).
22. C. Arpesella *et al.*, Phys. Lett. B **389**, 452 (1996).
23. Krauss *et al.*, Nucl. Phys. A **467**, 273 (1987).
24. T. Itahaschi *et al.*, Nucl. Phys. A **718**, 466c (2003).
25. D. Tilley *et al.*, Nucl. Phys. A **708**, 3 (2002).
26. J. Osborne *et al.*, Phys. Rev. Lett. **48**, 1664 (1982).
27. H. Krawinkel *et al.*, Z. Phys. A **304**, 307 (1982).
28. H. Holmgren, R. Johnston, Phys. Rev. **113**, 1556 (1959).
29. P. Parker, R. Kavanagh, Phys. Rev. **131**, 2578 (1963).
30. K. Nagatani, M.R. Dwarakanath, D. Ashery, Nucl. Phys. A **128**, 325 (1969).
31. Alexander *et al.*, Nucl. Phys. A **427**, 526 (1984).
32. M. Hilgemeier *et al.*, Z. Phys. A **329**, 243 (1988).
33. A. Kontos *et al.*, Phys. Rev. C **87**, 065804 (2013).
34. R.G.H. Robertson *et al.*, Phys. Rev. C **27**, 11 (1983).
35. H. Volk *et al.*, Z. Phys. A **310**, 91 (1983).
36. B.S. Nara Singh, M. Hass, Y. Nir-El, G. Haquin, Phys. Rev. Lett. **93**, 262503 (2004).
37. M. Carmona-Gallardo *et al.*, Phys. Rev. C **86**, 032801 (2012).
38. C. Bordeanu *et al.*, Nucl. Phys. **908**, 1 (2013).
39. T.A.D. Brown *et al.*, Phys. Rev. C **76**, 055801 (2007).
40. M. Nessin, T.H. Kruse, K.E. Eklund, Phys. Rev. **125**, 639 (1962).
41. S. Burles, K.M. Nollett, J.W. Truran, M.S. Turner, Phys. Rev. Lett. **82**, 4176 (1999).
42. P. Serpico, S. Esposito, F. Iocco, G. Mangano, G. Miele, O. Pisanti, JCAP **12**, 010 (2004).
43. A. Formicola *et al.*, Nucl. Instrum. Methods Phys. Res. A **507**, 609 (2003).
44. H. Costantini *et al.*, Nucl. Phys. A **814**, 144 (2008).
45. F. Confortola *et al.*, Phys. Rew. C **75**, 065803 (2007).
46. C. Casella *et al.*, Nucl. Instrum. Methods Phys. Res. A **489**, 160 (2002).
47. A. Caciolli *et al.*, Eur. Phys. J. A **39**, 179 (2009).
48. A. Best *et al.*, Eur. Phys. J. A **51**, 72 (2016) contribution to this Topical Issue.
49. D. Bemmerer *et al.*, Phys. Rev. Lett. **97**, 122502 (2006).
50. T.A. Tombrello, P.D. Parker, Phys. Rev. A **131**, 2582 (1963).
51. B.T. Kim, T. Izumoto, K. Nagatani, Phys. Rev. C **23**, 33 (1981).
52. S. Agostinelli *et al.*, Nucl. Instrum. Methods A **506**, 250 (2003).
53. M.H. Mendenhall, R.A. Weller, Nucl. Instrum. Methods B **227**, 420 (2005).
54. C. Arpesella *et al.*, Appl. Radiat. Isot. **47**, 991 (1996).
55. G. Gyurky *et al.*, Phys. Rev. C **75**, 035805 (2007).
56. H. Assenbaum, K. Langanke, C. Rolfs, Z. Phys. A **327**, 461 (1987).
57. P. Prati *et al.*, Z. Phys. A **621**, 452 (1997).
58. R.J. deBoer *et al.*, Phys. Rev. C **90**, 035804 (2014).
59. A. Di Leva *et al.*, Phys. Rev. Lett. **102**, 232502 (2009).
60. A. Formicola *et al.*, Phys. Lett. B **591**, 61 (2004).
61. G. Imbriani *et al.*, Eur. Phys. J. A **25**, 455 (2005).
62. A. Lemut *et al.*, Phys. Lett. B **634**, 483 (2006).
63. D. Bemmerer *et al.*, Nucl. Phys. A **779**, 297 (2006).
64. M. Marta *et al.*, Phys. Rev. C **78**, 022802(R) (2008).
65. R.C. Runkle *et al.*, Phys. Rev. Lett. **94**, 082503 (2005).
66. P.F. Bertone *et al.*, Phys. Rev. Lett. **87**, 152501 (2001).
67. A.M. Mukhamedzhanov *et al.*, Phys. Rev. C **67**, 065804 (2003).
68. S.O. Nelson *et al.*, Phys. Rev. C **68**, 065804 (2003).
69. D. Schurmann *et al.*, Phys. Rev. C **77**, 055803 (2008).
70. K. Yamada *et al.*, Phys. Lett. B **579**, 265 (2004).
71. U. Schröder *et al.*, Nucl. Phys. A **467**, 240 (1987).
72. C. Angulo, P. Descouvemont, Nucl. Phys. A **690**, 755 (2001).
73. G. Imbriani *et al.*, Astron. Astrophys. **420**, 625 (2004).
74. S. Deg'Innocenti *et al.*, astro-ph/0312559.
75. R.E. Azuma *et al.*, Phys. Rev. C **81**, 045805 (2010).
76. A. Serenelli, C. Pena-Garay, W.C. Haxton, Phys. Rev. D **87**, 043001 (2013).
77. W.C. Haxton, A.M. Serenelli, Astrophys. J. **687**, 678 (2008).
78. N. Grevesse, A.J. Sauval, Space Sci. Rev. (1998).
79. A. Serenelli, *Alive and well: A short review about standard solar models*, contribution to this Topical Issue, arXiv:1601.07179.